Layer-by-layer shuttered molecular-beam epitaxial growth of superconducting Sr1–x Lax CuO2 thin films

L. Maritato, A. Galdi, P. Orgiani, J. W. Harter, J. Schubert, K. M. Shen, and D. G. Schlom

___

Articles you may be interested in

Effect of superconducting spacer layer thickness on magneto-transport and magnetic properties of La0.7Sr0.3MnO3/YBa2Cu3O7/La0.7Sr0.3MnO3 heterostructures
J. Appl. Phys. **115**, 013901 (2014); 10.1063/1.4861139

Superconducting epitaxial thin films of CeNi x Bi 2 with a bismuth square net structure
Appl. Phys. Lett. **101**, 162602 (2012); 10.1063/1.4760264

Irreversibility line and thermally activated flux flow in La 1.6 − x Nd 0.4 Sr x CuO 4 films
J. Appl. Phys. **99**, 053903 (2006); 10.1063/1.2174120

Electron-doped infinite-layer thin films with T C over 40 K grown on DyScO 3 substrates
Appl. Phys. Lett. **84**, 2136 (2004); 10.1063/1.1688979

Single-crystalline superconducting thin films of electron-doped infinite-layer compounds grown by molecular-beam epitaxy
Appl. Phys. Lett. **79**, 2767 (2001); 10.1063/1.1410872

___

Layer-by-layer shuttered molecular-beam epitaxial growth of superconducting $Sr_{1-x}La_xCuO_2$ thin films

L. Maritato,[1,2,a)] A. Galdi,[1] P. Orgiani,[1] J. W. Harter,[3] J. Schubert,[4] K. M. Shen,[3,5] and D. G. Schlom[2,5]

[1]*Dipartimento di Ingegneria dell'Informazione, Ingegneria Elettrica e Matematica Applicata-DIEM,University of Salerno and CNR-SPIN, 84084 Fisciano (SA), Italy*
[2]*Department of Materials Science and Engineering, Cornell University, Ithaca, New York 14853, USA*
[3]*Laboratory of Atomic and Solid State Physics, Department of Physics, Cornell University, Ithaca, New York 14853, USA*
[4]*Forschungszentrum Julich, Institute of Bio- and Nano-systems IBN, D-52425 Julich, Germany and Forschungszentrum Julich, JARA Fundamentals of Future Information Technology, D-52425 Julich, Germany*
[5]*Kavli Institute at Cornell for Nanoscale Science, Ithaca, New York 14853, USA*

Superconducting $Sr_{1-x}La_xCuO_2$ thin films have been grown on $GdScO_3$ substrates by reflection high-energy electron diffraction calibrated layer-by-layer molecular-beam epitaxy. X-ray diffraction analysis has confirmed the infinite layer structure after an *in situ* vacuum annealing step. *In situ* photoemission spectroscopy indicates that the vacuum annealing step employed immediately after film growth to achieve superconducting films results in oxygen loss from the films. The superconducting critical temperature depends on the La content x, with the highest value obtained for $x \sim 0.10$. Resistivity as a function of temperature $\rho(T)$ curves of optimally doped samples show a T^2 temperature dependence characteristic of a scattering process where electron-electron interactions dominate. © 2013 American Institute of Physics. [http://dx.doi.org/10.1063/1.4790150]

I. INTRODUCTION

The $ACuO_2$ *infinite-layer* (IL) compounds, where CuO_2 sheets with four-fold Cu atoms coordinated by O are separated by Ca and/or Sr cations (A), have the simplest structure of all known superconducting cuprates.[1,2] In spite of this structural simplicity, bulk synthesis of superconducting ILs presents many difficulties (particularly for $SrCuO_2$), requiring the use of high-pressure techniques.[3,4] Partial substitution of large rare-earth (RE) 3+ ions (La, Pr, Nd, Sm, Gd) for Sr^{2+} produces n-type superconducting compounds with a maximum critical temperature T_c around 43 K.[5,6] IL materials, along with the $RE_{2-x}Ce_xCuO_4$ compounds (maximum T_c around 30 K (Refs. 7 and 8)), are the two most investigated materials showing electron-doped high temperature superconductivity.[9] Several groups have grown doped IL thin films by various deposition techniques[10–17] (molecular-beam epitaxy (MBE), laser ablation, sputtering) to study their superconducting properties. To obtain good superconducting IL films, the use of suitable substrates is critical.[10,11] The biaxial strain induced by the substrate plays an important role in determining the Cu-O coordination number, e.g., the presence or absence of apical oxygen. In particular, while compressive in-plane epitaxial strain (as in the case of $SrTiO_3$ substrates) generally gives IL films with inferior superconducting performances,[13–15] in-plane tensile strain ($KTaO_3$ and $DyScO_3$ substrates) produces IL superconducting films with critical temperatures close to the bulk value and with low metallic resistivities.[10–12,17]

Reflection high-energy electron diffraction (RHEED) assisted layer-by-layer MBE, with its ability to control growth at the level of single atomic planes, is an excellent technique for fabricating IL layered systems. Very good superconducting IL thin films have been produced by co-deposition MBE,[10,11] while (probably due to the use of $SrTiO_3$ substrates) IL samples with inferior superconducting properties have been obtained by RHEED-assisted layer-by-layer MBE.[12] Here we report the growth of IL epitaxial $Sr_{1-x}La_xCuO_2$ thin films on $GdScO_3$ (110) substrates with superconducting critical temperatures as high as 35 K by using shuttered MBE. In addition to measuring the transport properties of the samples, they have been investigated by *in situ* photoemission spectroscopy. The ability to fabricate n-type superconducting IL films with this layer-by-layer technique provides a way to study interface effects in heterostructures based on this class of materials.

II. SAMPLE PREPARATION

$Sr_{1-x}La_xCuO_2$ films were grown in a Veeco GEN10 dual-chamber oxide MBE system using a shuttered layer-by-layer deposition process performed in purified O_3 at a background pressure of 1×10^{-6} Torr. The films were deposited on $GdScO_3$ (110) substrates which have a distorted perovskite structure with a pseudo-cubic lattice constant of 0.3968 nm.[18] During growth, the substrate temperature T_s, as measured by a thermocouple and pyrometer, was in the range 500-550 °C. Immediately following film growth, the samples were vacuum annealed *in situ* (typically around 10^{-8} Torr) at temperatures typically a few degrees higher than T_s for 30 min and then cooled to room temperature in vacuum. This annealing step

a)Author to whom correspondence should be addressed. Electronic mail: lmaritato@unisa.it.
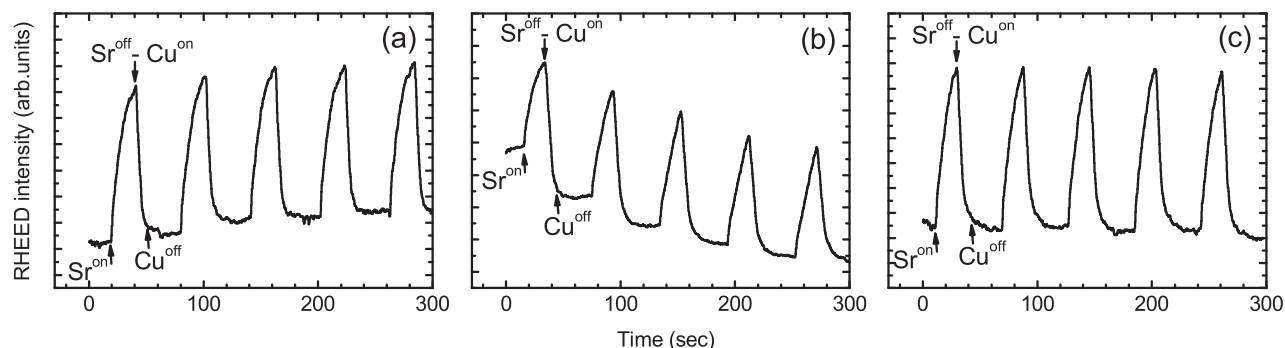
FIG. 1. Time dependence of the [01] diffraction rod intensity of a typical RHEED pattern during calibration for the case of (a) Sr-rich layers, (b) Cu-rich layers, and (c) with the Sr/Cu ratio close to 1. In each panel, the first opening Cu^{on}-Sr^{on} and closing Cu^{off}-Sr^{off} times of the Cu/Sr shutters are indicated by arrows.

was crucial for obtaining superconductivity. The Sr and Cu shutter opening times were calibrated by monitoring RHEED oscillations during the growth of undoped SrCuO$_2$ films. The RHEED patterns were taken with a glancing electron beam parallel to one of the in-plane $[100]_p$ azimuths of the substrate, where the subscript p indicates pseudocubic indices. Figures 1(a) and 1(b) show the time dependence of the [01] diffraction rod intensity for the case of Sr (Cu) rich layers.

With opening times adjusted so that the Sr/Cu ratio is close to 1, the RHEED oscillations are constant in intensity, as shown in Fig. 1(c). When depositing many ABO_3 perovskite-like compounds using layer-by-layer MBE, oscillations are known to show beating effects if the shuttered A and B atomic monolayers are incomplete.[19,20] In the case of undoped IL thin films, we have never observed such beating effects. We have therefore used the values of the c-axis lattice constant and of the total film thickness, both measured by x-ray diffraction analysis, to compare the number of shuttering periods to that of the actual number of unit cells present along the growth direction in our calibration samples. The equality between these two values is indicative of perfectly alternating complete Sr and Cu-O$_2$ monolayers. After this calibration of the Sr and Cu shutter opening times, the layer-by-layer growth of a Sr$_{1-x}$La$_x$CuO$_2$ thin film is achieved by opening and closing the La shutter simultaneously with the Sr shutter. The La shutter opening time is determined by measuring the La flux via a quartz crystal monitor (QCM). The actual doping level of the films was checked by Rutherford backscattering spectrometry (RBS) which was found to always match the QCM value of x in Sr$_{1-x}$La$_x$CuO$_2$ to within ± 0.01.

In Fig. 2(a), a typical RHEED pattern at the end of the growth is shown. An extra diffraction streak between the [01] and [02] diffraction rods is present in Fig. 2(a), but disappears after the first few minutes of the vacuum annealing step, Fig. 2(b). The same extra diffraction streak (arrowed in Fig. 2(a)) also periodically appeared during the layer-by-layer growth at the completion of each Cu monolayer, and disappeared with the deposition of the following Sr monolayer. Similar extra streaks observed in the case of layer-by-layer MBE deposited undoped IL thin films[21] have been used to calibrate the Sr (Cu) monolayer growth. In our case, such a calibration procedure gave thin films where the number of shuttering periods was not equal to the number of unit cells grown, as calculated by x-ray diffraction analysis. Similar extra streaks

have also been observed in layer-by-layer pulsed-laser deposited IL thin films and have been ascribed to the presence of a loosely bonded Cu-rich overlayer which may subsequently react with incident Sr atoms to form the epitaxial IL structure.[13] The strong influence of vacuum annealing on these streaks suggests that oxygen plays a major role in their existence. *In situ* low-energy electron diffraction (LEED) analysis performed after the vacuum annealing step indicates that the structure of our IL films is composed of perfectly square and flat CuO$_2$ sheets, with surfaces of high quality and with no evidence of reconstruction.[22]
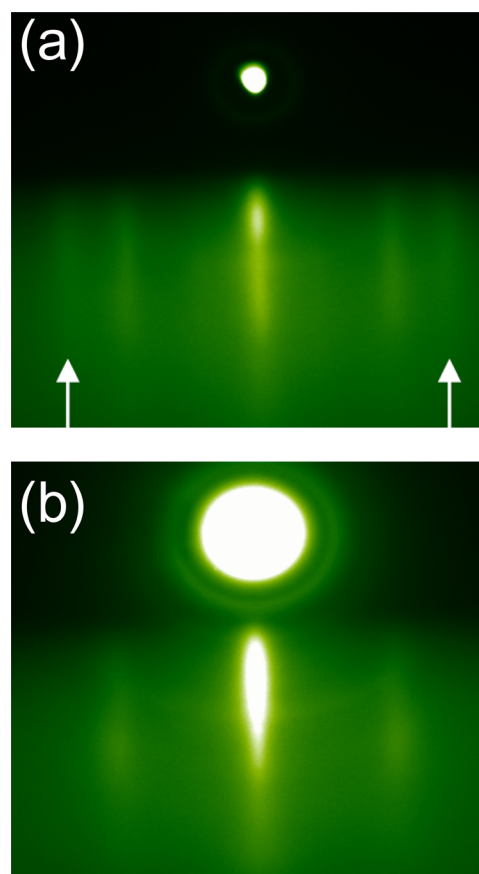

FIG. 2. Typical RHEED pattern of a (001) Sr$_{1-x}$La$_x$CuO$_2$ epitaxial thin film viewed along the $[110]_p$ azimuth (a) at the end of the growth, and (b) after the vacuum annealing step. Note the presence of the extra (arrowed) streak in (a), which vanishes during the vacuum annealing step (b).
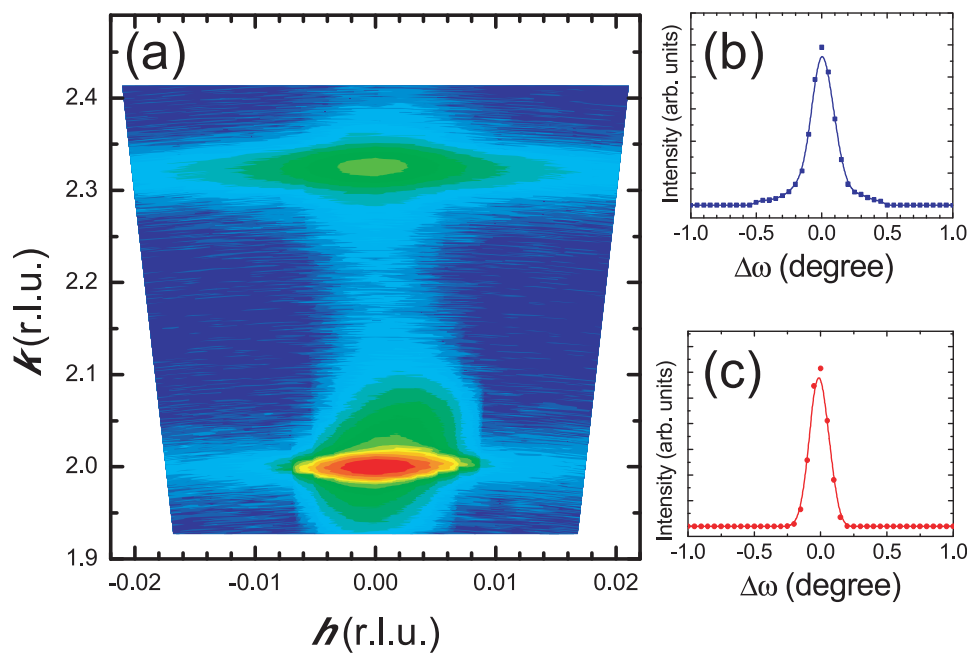
FIG. 3. (a) Reciprocal space map along h and k of a $Sr_{0.9}La_{0.1}CuO_2$ film grown on a (110) $GdScO_3$ substrate around the symmetric 002_p Bragg reflections (the units of h and k are those of the $GdScO_3$ pseudocubic reciprocal lattice). Rocking curves of the 002_p reflections of the film ((b) blue curve) and of the substrate ((c) red curve).

III. RESULTS AND DISCUSSION

X-ray diffraction (XRD) was performed on all deposited samples. In Fig. 3, we present an XRD reciprocal space map along h and k around the 002_p symmetric reflections of a 20 nm thick $Sr_{0.9}La_{0.1}CuO_2$ film grown on $GdScO_3$ (110).

The reciprocal space map only contains 002_p peaks, indicating the preferential c-axis orientation of the film along the $[001]_p$ substrate crystallographic direction. No sign of any secondary phase was seen by XRD. The c-axis parameter is calculated to be 0.340 ± 0.001 nm, in agreement with the expected value for apical-oxygen-free strained $Sr_{0.9}La_{0.1}CuO_2$ (Ref. 11) (within experimental error). In order to check the crystalline quality of the films, rocking curve measurements (ω-scans) were also performed (Figs. 3(b) and 3(c)). From the very close values of the full width at half-maximum (FWHM) of the film and the substrate, $0.185° \pm 0.004°$ and $0.133° \pm 0.007°$, respectively, the film can be deduced to be commensurately strained to the underlying substrate.[23] Such a strain condition has been confirmed by asymmetric XRD measurements of the 103 Bragg reflection, showing a peak at $2\theta = 89.89°$, corresponding to an a-axis parameter of 0.397 ± 0.002 nm.

To study the effect of the vacuum annealing process, *in situ* photoemission spectroscopy using He-Iα light (21.2 eV) was performed on both as-grown and vacuum annealed $Sr_{0.90}La_{0.10}CuO_2$ films. As Fig. 4 shows, a significant change in the O $2p$-derived valence band is observed after the vacuum annealing step. In particular, the leading edge of the valence band at ~ 2 eV shifts toward higher binding energies after annealing. This is consistent with electron-doping of the film via the removal of excess oxygen atoms, which, when present, accept electrons. In addition, the marked change in the spectral weight of the valence band suggests an entirely different electronic structure for the as-grown film, beyond a simple doping picture. Annealed samples show slight variations in the shape of the valence band spectrum, but are qualitatively similar to that presented in Fig. 4.

In Fig. 5, the electrical resistivity as a function of temperature is shown for three representative $Sr_{1-x}La_xCuO_2$ samples with different La doping levels. The resistivities in the figure are normalized to the room temperature values and are in the range 0.1-0.2 mΩ cm for all films. These resistivity measurements were performed using a van der Pauw four-probe geometry without patterning the samples. The highest superconducting critical temperature, $T_c = 35 \pm 1$ K,[24] was observed in the sample with La content $x = 0.1$. T_c decreases to a value of 28 ± 1 K for the underdoped sample with $x = 0.08$, and to 20 ± 1 K in the case of the over-doped film with $x = 0.13$. Along with the absolute value of T_c, remarkable differences arise among the samples in the normal-state resistance. Indeed, the temperature dependence of the resistivity curve provides insights into the basic transport mechanism at play in the system. In contrast with hole-doped cuprates, several studies have shown a T^2 power law dependence of $\rho(T)$ in electron-doped cuprates
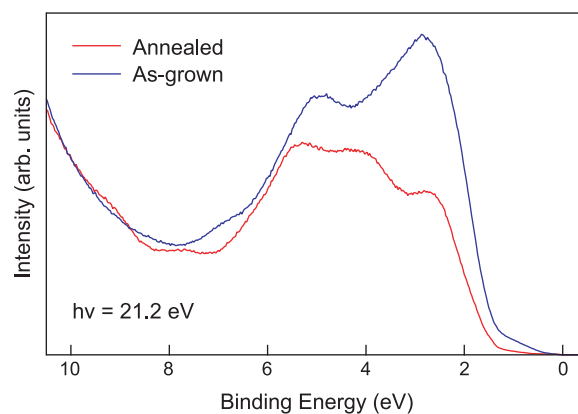

FIG. 4. *In situ* photoemission spectroscopy using He-Iα light (21.2 eV) showing the O $2p$-derived valence band in as-grown (blue) and vacuum annealed (red) $Sr_{0.90}La_{0.10}CuO_2$ films. A significant change in the valence band is observed after vacuum annealing, indicating electron-doping via the removal of excess electron-accepting oxygen atoms. The spectra have been normalized at high binding energy (~ 10 eV).
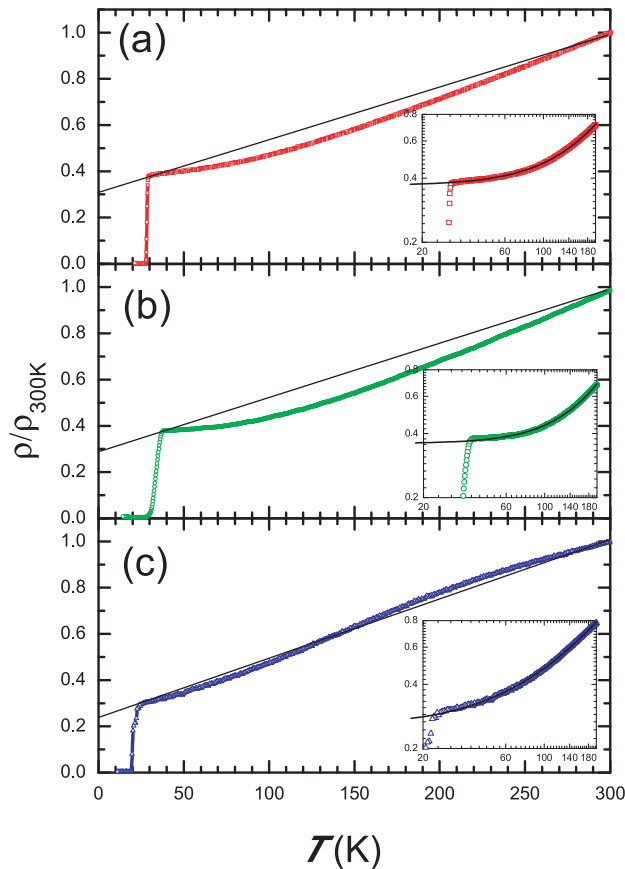
FIG. 5. Room temperature normalized resistivity curves for three $Sr_{1-x}La_x$ CuO_2 samples with different La concentrations. Data refer to films with La content x equal to 0.08 (red squares, (a)), 0.10 (green circles, (b)) and 0.13 (blue triangles, (c)). Straight lines are guides to the eye. Insets show low-temperature resistivity and corresponding best-fit curves using a log-log scale.

over a wide temperature range (up to 250 K),[9,25] rather than the linear dependence observed in the hole-doped cuprates. Such results point to a conventional metallic electron-electron scattering mechanism for optimally doped n-type superconducting cuprates rather than a phonon-driven contribution to resistivity or the presence of a pseudogap usually associated with a linear-scaling behavior of the resistivity.[26] As is clearly evident from the data in Fig. 5, none of the samples show a linear temperature dependence of the resistivity. In analogy with high-temperature cuprates,[27,28] an up(down)ward curvature in the resistivity curves has been observed for underdoped (overdoped) samples. Such a transition is, however, so abrupt that a linear scaling law has never been observed despite the large number of samples investigated.

In order to shed light on the transport properties of electron-doped IL compounds, we fit the resistivity curves $\rho(T)$ using a generic T^n power law, as has been done for other strongly correlated systems.[25,29,30] This power law can simulate different scattering processes and help to reveal the most active scattering channel.[31] More precisely, in the normal-state phase, the $\rho(T)$ curves can be best fit by the formula $\rho(T) = \rho_0 + A\,T^n$, where A and n are free parameters. We have varied the fitting temperature range in units of 10 K, keeping the lowest temperature fixed (3 K higher than the

onset of the superconducting transition). As the temperature range increases, the statistical error on the fitting parameters monotonically decreases, while the reduced χ^2 value remains unchanged (in the range of 10^{-6}), until a critical range is reached at which both the χ^2 and the statistical errors abruptly change (both by over one order of magnitude). For all of the samples, such a critical point was found near 150 K.

The resistivity curve of the optimally doped SLCO sample scales very well as T^n with $n = 2.08$, quite close to the value of 2 which is characteristic of a predominant electron-electron scattering process at low temperatures as previously observed in electron-doped cuprates.[25] Both the underdoped and overdoped samples, however, show a value of n far from that observed in the optimally doped system (namely, n is 1.78 and 1.39 for underdoped and overdoped samples, respectively). Such values cannot be easily associated with one specific scattering mechanism, but are most probably related to more complex transport mechanisms.[30]

IV. CONCLUSIONS

In conclusion, we have grown superconducting $Sr_{1-x}La_x$ CuO_2 films using a shuttered layer-by-layer MBE technique. The controlled deposition of single monoatomic layers has been achieved via RHEED calibration. The *in situ* post deposition vacuum annealing step, which is critical for obtaining superconducting IL single phase samples, results in a shorter c-axis length as revealed by XRD and oxygen loss according to *in situ* photoemission spectroscopy. The superconducting critical temperatures vary with the La stoichiometry x, with the highest value obtained when $x \sim 0.1$. Analysis of the transport properties of optimally doped samples reveals a T^2 dependence of the $\rho(T)$ curves, typically associated with electron-electron scattering mechanisms. In the case of over-doped samples, the curvature of the ρ vs. T curve shows the expected high-temperature downward behavior. The ability of shuttered MBE, which controls and varies the atomic species in a single atomic monolayer of IL epitaxial thin films, opens new exciting perspectives in the fabrication of functional heterostructures based on this class of compounds.

[1]T. Siegrist, S. M. Zahurak, D. W. Murphy, and R. S. Roth, Nature **334**, 231 (1988).
[2]R. J. Cava, Nature **351**, 518 (1991).
[3]M. G. Smith, A. Manthiram, J. Zhou, J. B. Goodenough, and J. T. Markert, Nature **351**, 549 (1991).
[4]Y. Tanaka, M. Karppinen, and H. Yamauchi, Supercond. Sci. Technol. **22**, 065004 (2009), and references therein.
[5]G. Er, Y. Miyamoto, F. Kanamaru, and S. Kikkawa, Physica C **181**, 206 (1991).
[6]N. Ikeda, Z. Hiroi, M. Azuma, M. Takano, Y. Bando, and Y. Takeda, Physica C **210**, 367 (1993).

[7]T. Yamada, K. Kinoshita, and H. Shibata, Jpn. J. Appl. Phys. Part 2 **33**, L168 (1994).

[8]M. Naito and M. Hepp, Jpn. J. Appl. Phys. Part 2 **39**, L485 (2000).

[9]N. P. Armitage, P. Fournier, and R. L. Greene, Rev. Mod. Phys. **82**, 2421 (2010).

[10]S. Karimoto, K. Ueda, M. Naito, and T. Imai, Appl. Phys. Lett. **79**, 2767 (2001).

[11]S. Karimoto and M. Naito, Appl. Phys. Lett. **84**, 2136 (2004).

[12]S. Oh and J. N. Eckstein, Thin Solid Films **483**, 301 (2005).

[13]V. Leca, D. H. A. Blank, G. Rijnders, S. Bals, and G. van Tendeloo, Appl. Phys. Lett. **89**, 092504 (2006).

[14]A. Gupta, B. W. Hussey, T. M. Shaw, A. M. Guloy, M. Y. Chern, R. F. Saraf, and B. A. Scott, J. Solid State Chem. **112**, 113 (1994).

[15]R. Feenstra, X. Li, M. Kanai, T. Kawai, S. Kawai, J. D. Budai, E. C. Jones, Y. R. Sun, J. R. Thompson, S. J. Pennycook, and D. K. Christen, Physica C **224**, 300 (1994).

[16]J. Tomashko, V. Leca, T. Selistrovski, S. Diebold, J. Jochum, R. Kleiner, and D. Koelle, Phys. Rev. B **85**, 024519 (2012).

[17]V. P. Jovanovic, Z. Z. Li, and H. Raffy, Supercond. Sci. Technol. **24**, 055002 (2011).

[18]R. Uecker, B. Velickov, D. Klimm, R. Bertram, M. Bernhagen, M. Rabe, M. Albrecht, R. Fornari, and D. G. Schlom, J. Cryst. Growth **310**, 2649 (2008).

[19]J. H. Haeni, C. D. Theis, and D. G. Schlom, J. Electroceram. **4**, 385 (2000).

[20]C. Adamo, A. Soukiassian, T. Heeg, C. M. Brooks, C. H. Lee, J. A. Mundy, Y. Nie, P. King, S. Zhu, L. Maritato, and D. G. Schlom, "In situ Composi-tion Control of Oxide Thin Films using Shuttered RHEED Intensity Oscil-lations" (unpublished).

[21]Z. Liu, T. Hanada, R. Sekine, M. Kawai, and H. Koinuma, Appl. Phys. Lett. **65**, 1717, (1994).

[22]J. W. Harter, L. Maritato, D. E. Shai, E. J. Monkman, Y. Nie, D. G. Schlom, and K. M. Shen, Phys. Rev. Lett. **109**, 267001 (2012).

[23]P. F. Miceli and C. J. Palmstrøm, Phys. Rev. B **51**, 5506 (1995).

[24]The superconducting critical temperature is defined as the point at which $\rho(T) = 0.5\rho_N$, with ρ_N the resistivity in the normal low temperature state immediately before the transition.

[25]C. C. Tsuei, A. Gupta, and G. Koren, Physica C **161**, 415 (1989).

[26]R. R. Daou, N. Doiron-Leyraud, D. LeBoeuf, S. Y. Li, F. Laliberté, O. Cyr-Choinière, Y. J. Jo, L. Balicas, J.-Q. Yan, J.-S. Zhou, J. B. Goode-nough, and L. Taillefer, Nat. Phys. **5**, 31 (2009).

[27]P. Orgiani, C. Aruta, G. Balestrino, D. Born, L. Maritato, P. G. Medaglia, D. Stornaiuolo, F. Tafuri, and A. Tebano, Phys. Rev. Lett. **98**, 036401 (2007).

[28]I. Bozovic, G. Logvenov, I. Belca, B. Narimbetov, and I. Sveklo, Phys. Rev. Lett. **89**, 107001 (2002).

[29]R. A. Cooper, Y. Wang, B. Vignolle, O. J. Lipscombe, S. M. Hayden, Y. Tanabe, T. Adachi, Y. Koike, M. Nohara, H. Tagagi, C. Proust, and N. E. Hussey, Science **323**, 603 (2009).

[30]K. Jin, N. P. Butch, K. Kirshenbaum, J. Paglione, and R. L. Green, Nature **476**, 73 (2011).

[31]P. Orgiani, C. Adamo, C. Barone, A. Galdi, A. Yu. Petrov, D. G. Schlom, and L. Maritato, Phys. Rev. B **76**, 012404 (2007).